

Ruize Xu\* and Sang-Gook Kim

# Modeling and Experimental Validation of Bi-Stable Beam Based Piezoelectric Energy Harvester

DOI 10.1515/ehs-2015-0022

**Abstract:** We have previously proposed a bi-stable nonlinear oscillator based piezoelectric energy harvester to address the challenges of low-frequency, low-g vibration energy harvesting at MEMS scale. The compressive residual stress in micro-fabricated thin films could be employed to induce buckling in doubly clamped beams. The buckled beams with two equilibriums can snap through at low frequencies and enhance the power generation. This paper focuses on the modeling of the dynamics of the bi-stable oscillator based energy harvesters. An electromechanical lumped model has been built by Lagrange's formulation and lumped parameters have been solved explicitly. More particularly, the model considers multi-layer thin films and the residual stress in these films, to be readily applicable to MEMS device design. Harmonic functions as the approximate solutions have been used to analytically solve for the frequency responses of the nonlinear oscillations. Two modes of oscillations predicted by the analytical model have been validated by testing a meso-scale prototype.

**Keywords:** bi-stable oscillator, modeling, micro-electro-mechanical systems, piezoelectricity, vibration energy harvester

## Introduction

Piezoelectric energy harvesting is an efficient way to convert kinetic energy of ambient vibrations into electrical power. Previous studies have achieved high output voltage, high output power density and wide bandwidth from MEMS piezoelectric energy harvesting (Hajati and Kim 2011). Challenges, however, still exist in applying this technology into real applications: the current devices require much higher input vibration frequency and

amplitude than those of the typical ambient vibrations. A new MEMS energy harvester, which could potentially lower the working frequency ( $<100$  Hz) and excitation amplitude ( $<1$  g), has been proposed previously (Xu and Kim 2015). The device is a  $12\text{ mm} \times 15\text{ mm}$  doubly clamped beam consisting of compressive  $\text{Si}_3\text{N}_4$ ,  $\text{SiO}_2$  layers and PZT patches. The simulation shows a wide working frequency range below 120 Hz at 1 g excitation.

Bi-stable nonlinear resonance has been investigated to increase the power bandwidth. The typical bi-stable designs are based on magnetic force (Mann and Owens 2010; Erturk and Inman 2011), mechanical compression (Jung and Yun 2010; Cottone et al. 2012), composites plate (Arrieta et al. 2010, 2013a; Betts et al. 2012, 2013), and pre-shaped beam (Qiu, Lang, and Slocum 2004). These approaches have shown that bi-stable nonlinear resonance widens the bandwidth of the energy harvesters as the mono-stable nonlinear resonance does. We have proposed utilizing pure mechanical bi-stability of a buckled beam to enhance energy generation at MEMS scale from low-frequency vibrations to eliminate the need of assembling magnets or applying manual compression. Our design is based on the common characteristics of micro-fabricated thin films – residual stress, which is typically in the order of  $10^1 \sim 10^2$  MPa. When the total stress in a beam is compressive and beyond the Euler buckling limit, the clamped-clamped beam will buckle, either upward or downward, so that the system becomes bi-stable. The dynamics changes dramatically from mono-stable nonlinear oscillator. Many previous theoretical works are on the modeling of the bi-stable oscillator based energy harvesters. In Inman (2011), a bi-stable *Duffing* oscillator with electromechanical coupling has been investigated, but the simulations are only in the time domain. Stanton, McGehee, and Mann (2010) has formulated a PZT patched cantilever beam harvester with magnetic force induced bi-stability. In Cottone et al. (2012), a buckled beam bi-stable energy harvester has been modeled, while the work's interest is solving the dynamic equations with stochastic excitations. Composites based bi-stable plates were modeled in Arrieta et al. (2013b) and Taki et al. (2015). Since our

\*Corresponding author: Ruize Xu, Mechanical Engineering Department, Massachusetts Institute of Technology, Cambridge, MA 02139, USA, E-mail: rzxu@mit.edu

Sang-Gook Kim, Mechanical Engineering Department, Massachusetts Institute of Technology, Cambridge, MA 02139, USA

new design is targeting to work at low frequencies with continuous harmonic vibrations, and it will be implemented by MEMS fabrication, we are developing the theoretical framework with an electromechanically coupled lumped model, which incorporates the multi-layer structure and residual stress, and solving analytically by harmonic balance to obtain the frequency response of the energy harvesters.

## Modeling and Simulation

### One Degree-of-Freedom Electromechanical Lumped Parameter Model

The energy harvester we are modeling has a clamped-clamped beam structure of a stack of thin films including structural layer, seed layer, piezoelectric layer and passivation layer (Figure 1(a)). A heavy proof mass is concentrated at the middle of the beam to capture the external vibration and excites the whole beam to vibrate out-of-plane. Piezoelectric elements work in  $d_{33}$  mode with top interdigitated electrodes, coupling the mechanical response with electrical domain. The multi-layer beam

is designed to buckle by incorporating the controlled compressive residual stress of the micro-fabricated thin films. Statically, the beam either buckles up or down (two equilibriums), and the dynamics becomes complex when the system is continuously excited in post-buckling regime. To capture the essential dynamics phenomena of the complex system, the beam vibration mode has been assumed so that a one degree-of-freedom model can be constructed. The nonhomogeneous beam structure has been taken into account by considering the different thickness and material properties of each layer. Furthermore, residual stress of each layer is built in as part of the stiffness of the beam to induce buckling. The electrical and mechanical domains are coupled with linear and nonlinear coupling, so that the generated electrical power can be calculated.

The lumped parameter model is formulated by *Lagrange's* method. In classical mechanics, the *Lagrangian* is defined as,

$$L = KE - PE \quad [1]$$

where  $KE$  is the kinetic energy of the system,  $PE$  is the potential of the system. In this energy harvester as in many other vibration energy harvesters, the proof mass is much heavier than the beam's distributed mass, so that

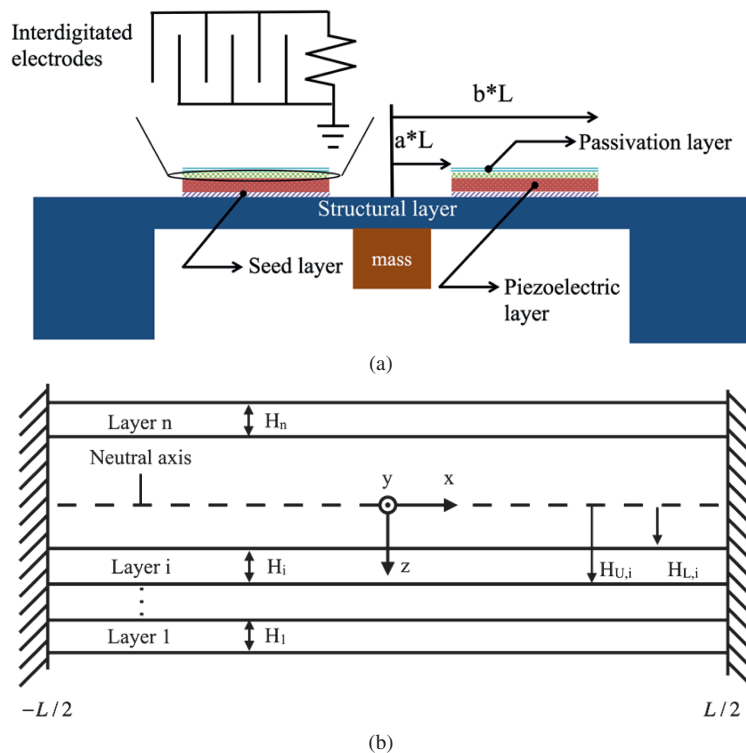


**Figure 1:** Schematics of the doubly clamped beam based energy harvester. (a) The piezoelectric element is in  $d_{33}$  mode with top interdigitated electrodes. The piezoelectric element and electrode span  $s$  symmetrically from  $-b \cdot L$  to  $-a \cdot L$  and  $a \cdot L$  to  $b \cdot L$  on the substrate. (b) The beam has  $n$  layers of different material thin films with various thicknesses.

the kinetic energy of the system is simplified as that of the center-concentrated proof mass,

$$KE = \frac{1}{2} m \dot{w}^2 \quad [2]$$

where  $m$  is the proof mass,  $\dot{w}$  is the time derivative of the beam center displacement, i. e. the velocity of the proof mass. To find out the thermodynamic potential of the system including the piezoelectric material, we start by considering the electrical enthalpy volume density:

$$\tilde{H}_e = \frac{1}{2} T_3 S_3 - \frac{1}{2} E_3 D_3 \quad [3]$$

and piezoelectric constitutive equations in  $d_{33}$  mode (Standards Committee of the IEEE Ultrasonics and Ferroelectrics 1988),

$$T_3 = c_{33}^E S_3 - E_3 e_{33} \quad [4]$$

$$D_3 = e_{33} S_3 + \epsilon_{33}^S E_3 \quad [5]$$

where  $T_3$ ,  $S_3$ ,  $D_3$ ,  $E_3$  are the stress, strain, electric displacement and electric field in 3-direction respectively;  $c_{33}^E$ ,  $e_{33}$  and  $\epsilon_{33}^S$  are the elastic modulus, piezoelectric constant, and permittivity of the piezoelectric material; the superscripts  $E$  and  $S$  denote the parameters are at constant electric field and strain respectively. Substitute  $T_3$  and  $D_3$  into [3], and add the strain energy contributed by the residual stress  $T_0$ ,  $\int_0^S T_0 ds = T_0 S_3$ :

$$\tilde{H}_e = \frac{1}{2} c_{33}^E S_3^2 - e_{33} E_3 S_3 - \frac{1}{2} \epsilon_{33}^S E_3^2 + T_0 S_3 \quad [6]$$

The residual stress in thin films micro-fabricated on a substrate causes a change in the radius of curvature of the substrate, which can be measured. The stress can then be calculated from the Stoney's formula:

$$T_0 = \frac{E_{sub} h_{sub}^2}{(1 - \nu_{sub}) 6 R t_{film}} \quad [7]$$

where  $E_{sub}$ ,  $\nu_{sub}$ ,  $h_{sub}$  are the Young's modulus, Poisson's ratio and thickness of the substrate,  $R$  is the substrate radius of curvature, and  $t_{film}$  is the thickness of the film. The *Lagrangian* of the system can now be evaluated by integrating the enthalpy density over the beam's volume layer by layer,

$$L = \frac{1}{2} m \dot{w}^2 - \sum_{i=1}^n \iiint_{V_i} \tilde{H}_{e,i} dv \quad [8]$$

where  $V_i$  is the volume of  $i$ -th layer and  $n$  is the total number of layers.

The strains developed in the beam need to be evaluated before carrying out the integrations in [9]. The total strain  $S_T$  developed in the beam has two components: bending strain, which changes linearly across the beam thickness, and axial strain due to large deflection,

$$S_T = -z \frac{d^2 \hat{w}}{dx^2} + \frac{1}{l} \int_{-L/2}^{L/2} \frac{1}{2} \left( \frac{d\hat{w}}{dx} \right)^2 dx \quad [9]$$

where  $l$  is the beam length. The strain is calculated from the neutral axis of the beam (Figure 1(b)). It should be stressed that the beam composes multilayers with various elastic properties, the neutral axis therefore does not coincide with the mid-plane. The general formula for calculating the position of the neutral axis (distance from the bottom surface) of a  $n$ -layer beam is,

$$h_{neutral} = \frac{\sum_{i=1}^n E_i H_i \sum_{j=1}^i H_j - \frac{1}{2} \sum_{i=1}^n E_i h_i^2}{\sum_{i=1}^n E_i h_i} \quad [10]$$

The beam vibrates up and down in  $z$ -axis, and by assuming that it vibrates predominantly in one mode, simplification can be made when evaluating the lumped parameters. The first buckling mode of the beam is adopted, which satisfies the boundary conditions of clamped-clamped beam and has been verified as the vibration mode shape at the largest deflection in experiment, by measuring the deflection on different spots along the beam using laser vibrometer (Figure 2). The deflection of the beam can then be separated into time and space,

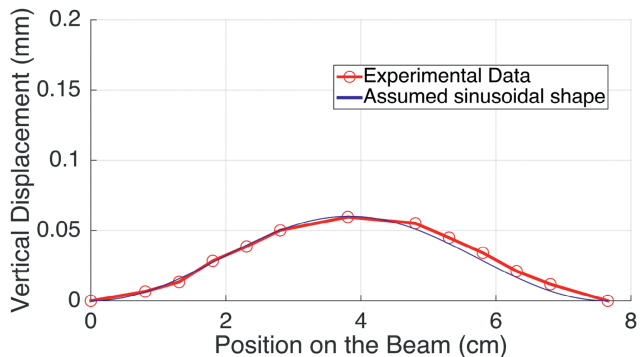


**Figure 2:** The comparison between measured maximum deflection versus the assumed sinusoidal function in [9]. The deflection was measured from single point laser vibrometer at various points on the vibrating beam. The assumed shape agrees well with the beam vibration shape.

$$\hat{w} = \frac{w(t)}{2} \left( 1 + \cos \frac{2\pi x}{l} \right) \quad [11]$$

where  $w(t)$  is the deflection of the beam center varying with time.

*Lagrange* equations are,

$$\frac{d}{dt} \left( \frac{\partial L}{\partial \dot{\xi}_i} \right) - \frac{\partial L}{\partial \xi_i} = Q_i^{Force} + Q_i^{Dissipation} \quad [12]$$

where  $\xi_i$  is the  $i$ -th independent generalized coordinate,  $Q_i^{Force}$  and  $Q_i^{Dissipation}$  are the generalized external force and the generalized dissipative force. We choose the deflection of the mid-point of the beam  $w$  and the output voltage  $V$  as the generalized coordinates. The *Lagrange* equation with respect to the first coordinate  $w$  is then,

$$\frac{d}{dt} \left( \frac{\partial L}{\partial \dot{w}} \right) - \frac{\partial L}{\partial w} = F - b\dot{w} \quad [13]$$

Evaluating the integrations in [8] and substituting into [13], the governing equation of the mechanical domain can be obtained and written in a compact form,

$$m\ddot{w} + k_L w + k_N w^3 + b\dot{w} + c_N w V_N + c_L V_L = F \quad [14]$$

where  $k_L$ ,  $k_N$ ,  $b$ ,  $c_L$ ,  $c_N$  and  $F$  are the linear stiffness and nonlinear stiffness of the beam, the mechanical damping coefficient, the linear and nonlinear electromechanical coupling, and the external excitation force respectively. These lumped parameters are functions of the device dimensions and material properties, which are useful for device design,

$$k_L = \left[ \frac{2\pi^4 W}{3l^3} \sum_{i=1}^n c_{33,i}^E (H_{U,i}^3 - H_{L,i}^3) \right] + \left[ \frac{\pi^2 W}{2l} \sum_{i=1}^n T_{0,i} H_i \right] \quad [15]$$

$$k_N = \frac{\pi^4 W}{8l^3} \sum_{i=1}^n c_{33,i}^E H_i \quad [16]$$

$$c_L = \frac{\pi e_{33} W (H_{U,p}^2 - H_{L,p}^2) (\sin(2\pi b) - \sin(2\pi a))}{lg} \quad [17]$$

$$c_N = \frac{\pi^2 e_{33} W H_p (b-a)}{lg} \quad [18]$$

where  $W$ ,  $H$ , are the width and thickness,  $a$  and  $b$  denotes the span of the electrodes on the beam, since they do not cover the whole beam (Figure 1(a)), and  $g$  is the gap between two electrode fingers; the subscript  $p$  denotes the variable is associated to the piezoelectric layer. It should be noted that the linear stiffness has two parts: the first part is from bending of the beam and the second comes from the residual stress. More particularly, when

the residual stress is negative (compressive) and large enough, the linear stiffness  $k_L$  will be negative, so that [14] becomes a characteristic bi-stable *Duffing* equation.

The second *Lagrange* equation with respect to the coordinate  $V$  is,

$$\frac{d}{dt} \left( \frac{\partial L}{\partial \dot{V}} \right) - \frac{\partial L}{\partial V} = \frac{\int V dt}{R} \quad [19]$$

Taking time derivative of the equation gives the governing equation for the electrical domain,

$$C_0 (\dot{V}_L + \dot{V}_N) + \frac{V_L + V_N}{R} = I_L + I_N \quad [20]$$

where  $I_L = c_L \dot{w}$  and  $I_N = c_N w \dot{w}$  are two parts of the electrical current generated by piezoelectric element through coupling, and  $L$  and  $N$  denote linear and nonlinear coupling respectively; the induced voltages on the electrical port are written in separate parts  $V_L$  and  $V_N$ , due to the fact that they come from two parts of the current respectively and have different frequencies due to different coupling, and this differentiation makes the assumptions on their function simple (next section).  $C_0$  is the internal capacitance of the piezoelectric element and is calculated as

$$C_0 = \frac{WH_p \epsilon_{33}^S}{g^2} \quad [21]$$

## Analytical Solution of the Frequency Response

The nonlinear governing equations [14] and [20] could be numerically integrated to obtain the solution in time domain, but analytical solutions provide more insights on the dynamic behavior; more importantly, the explicit relations between system parameters and the performance are significant for device design. Therefore, the heuristic harmonic balance method is adopted to approximate the frequency response analytically.

Bi-stable oscillator has characteristic double-well potential (Xu and Kim 2015). Depending on if the oscillator has enough energy to overcome the energy barrier, it crosses the well and has the so called inter-well oscillation, or stays in one well and oscillates intra-well. To differentiate the two modes of oscillations, we assumed that when the beam oscillates around the buckled configuration (intra-well), the beam is oscillating around a non-zero bias position  $\delta$  from the flat position; while the bias  $\delta$  is zero, the beam oscillates around the flat position and the oscillation becomes symmetric on both sides of the flat position (inter-well). Consider the intra-well case first: plug



in the assumed functions of  $w$  to [14], and balance the terms with  $\delta$  but without sinusoidal functions, we find  $\delta$ , which is a function of the deflection amplitude,

$$\delta = \sqrt{-\frac{k_L}{k_N} - \frac{3}{2}w_0^2} \quad [22]$$

By assuming the external force is sinusoidal and continuous, from trigonometric relations, it is easily found that the frequency of the induced electrical current from nonlinear coupling doubles that of the current from linear coupling. Physically, it is due to the developed stretching strain has half the cycle of the bending strain. The induced electrical current and voltage are then written in different parts with different frequencies shown in Table 1. The subscript  $0$  denotes amplitude. Unknown phase differences have been added to the sinusoidal functions and will be solved. Writing [20] into two separate equations, we can solve for  $V_L$  and  $V_N$  separately:

$$C_0 \dot{V}_L + \frac{V_L}{R} = c_L \dot{w} \quad [23]$$

$$C_0 \dot{V}_N + \frac{V_N}{R} = c_N w \dot{w} \quad [24]$$

Multiply [23] and [24] by  $\sin(\omega t)$  and  $\cos(\omega t)$ , integrate from  $0$  to  $2\pi$  and set both to zeros, we obtain six equations; and multiply [24] by  $\sin(2\omega t)$  and  $\cos(2\omega t)$ , integrate from  $0$  to  $\pi$  and set both to zeros, we obtain another four equations. Solving the ten equations, the amplitudes of voltages and the phase constants can be found,

$$V_{0,L} = \frac{c_L R \omega}{\sqrt{1 + C_0^2 R^2 \omega^2}} w_0 \quad [25]$$

$$V_{0,N}/V_{0,N1} = \frac{c_N R \omega}{2\sqrt{1 + 4C_0^2 R^2 \omega^2}} w_0^2 \quad [26]$$

$$V_{0,N2} = \frac{c_N R \omega w_0}{\sqrt{2 + 2C_0^2 R^2 \omega^2}} \cdot \sqrt{-\frac{2k_L}{k_N} - 3w_0^2} \quad [27]$$

$$\sin(\alpha) = \frac{C_0 R \omega}{\sqrt{1 + C_0^2 R^2 \omega^2}}, \quad \cos(\alpha) = \frac{1}{\sqrt{1 + C_0^2 R^2 \omega^2}} \quad [28]$$

$$\sin(\beta) = \frac{2C_0 R \omega}{\sqrt{1 + 4C_0^2 R^2 \omega^2}}, \quad \cos(\beta) = \frac{1}{\sqrt{1 + 4C_0^2 R^2 \omega^2}} \quad [29]$$

It is interesting to note that the voltage due to nonlinear coupling is a function of the deflection amplitude squared, while the voltage due to linear coupling is proportional to the deflection amplitude. This indicates that when the deflection is beyond some point, the nonlinear response will dominate the total response. The deflection amplitude is not known yet and will be solved from the mechanical domain equation [14].

Substitute assumed functions listed in Table 1 to [14], multiply by  $\sin(\omega t)$ , integrate from  $0$  to  $2\pi$ , set to zero, and multiply  $\cos(\omega t)$ , integrate from  $0$  to  $2\pi$ , set to zero, we obtain two equations:

$$f_1 w_0^3 + f_2 w_0 = F_0 \cos(\phi) \quad [30]$$

$$f_3 w_0^3 + f_4 w_0 = F_0 \sin(\phi) \quad [31]$$

Take the square of both sides of [30] and [31] and add them together, one equation with one unknown  $w_0$  is formed,

$$(f_1^2 + f_3^2) w_0^6 + 2(f_1 \cdot f_2 + f_3 \cdot f_4) w_0^4 + (f_2^2 + f_4^2) w_0^2 - f_5 = 0 \quad [32]$$

where  $f_1, f_2, f_3, f_4, f_5$  are functions of the known system's parameters:

$$f_1 = \frac{\left( -\frac{15}{4} k_N - c_N^2 C_0 R^2 \omega^2 - \frac{75}{4} C_0^2 k_N R^2 \omega^2 \right) - \frac{11}{2} C_0^3 c_N^2 R^4 \omega^4 - 15 C_0^4 k_N R^4 \omega^4}{(1 + C_0^2 R^2 \omega^2)(1 + 4C_0^2 R^2 \omega^2)} \quad [33]$$

$$f_2 = \frac{\left[ -m\omega^2 - 2k_L + c_L^2 C_0 R^2 \omega^2 - 10C_0^2 k_L R^2 \omega^2 - C_0 c_N^2 k_L R^2 \omega^2 / k_N - 5C_0^2 m R^2 \omega^4 + 4C_0^3 c_L^2 R^4 \omega^4 - 8C_0^4 k_L R^4 \omega^4 - 4C_0^3 c_N^2 k_L R^4 \omega^4 / k_N - 4C_0^4 m R^4 \omega^6 \right]}{(1 + C_0^2 R^2 \omega^2)(1 + 4C_0^2 R^2 \omega^2)} \quad [34]$$

**Table 1:** Assumed parameters expressions.

| Parameters                  | Assumed functions   |
|-----------------------------|---|
| Input force <sup>a</sup>    | $F = F_0 \sin(\omega t + \phi) = m \cdot a \sin(\omega t + \phi)$   |
| Beam mid-point displacement | $w = \delta + w_0 \sin(\omega t)$   |
| Current (inter-well)        | $I = I_L + I_N = I_{0,L} \cos(\omega t) + I_{0,N} \sin(2\omega t)$  |
| Current (intra-well)        | $I = I_L + I_N = I_{0,L} \cos(\omega t) + I_{0,N1} \sin(2\omega t) + I_{0,N2} \cos(\omega t)$                           |
| Voltage (inter-well)        | $V = V_L + V_N = V_{0,L} \cos(\omega t - \alpha) + V_{0,N} \sin(2\omega t - \beta)$                                     |
| Voltage (intra-well)        | $V = V_L + V_N = V_{0,L} \cos(\omega t - \alpha) + V_{0,N1} \sin(2\omega t - \beta) + V_{0,N2} \cos(\omega t - \alpha)$ |

Note: <sup>a</sup> $m$  and  $a$  are the proof mass and excitation amplitude (acceleration amplitude of vibrations).

$$f_3 = -\frac{3c_N^2 R\omega}{2(1+C_0^2 R^2 \omega^2)} + \frac{c_N^2 R\omega}{4(1+4C_0^2 R^2 \omega^2)} \quad [35]$$

$$f_4 = b\omega + \frac{c_L^2 R\omega}{1+C_0^2 R^2 \omega^2} - \frac{c_N^2 k_L R\omega}{k_N(1+C_0^2 R^2 \omega^2)} \quad [36]$$

$$f_5 = (m \cdot a)^2 \quad [37]$$

The inter-well oscillation is symmetric with respect to the flat unbuckled position, and hence there is no bias in  $w(t)$ . Solve [14], [23] and [24] in the same way as solving for the intra-well case, but with  $\delta = 0$ , we obtain the same equation as [32], but with different coefficients:

$$f_1 = \frac{3}{4}k_N + \frac{C_0 c_N^2 R^2 \omega^2}{2(1+4C_0^2 R^2 \omega^2)} \quad [38]$$

$$f_2 = -m\omega^2 + k_L + \frac{C_0 c_L^2 R^2 \omega^2}{1+C_0^2 R^2 \omega^2} \quad [39]$$

$$f_3 = \frac{c_N^2 R\omega}{4(1+4C_0^2 R^2 \omega^2)} \quad [40]$$

$$f_4 = b\omega + \frac{c_L^2 R\omega}{1+C_0^2 R^2 \omega^2} \quad [41]$$

$$V_{0,L} = \frac{c_L R\omega}{\sqrt{1+C_0^2 R^2 \omega^2}} w_0 \quad [42]$$

$$V_{0,N} = \frac{c_N R\omega}{2\sqrt{1+4C_0^2 R^2 \omega^2}} w_0^2 \quad [43]$$

[32] is an algebraic equation and is straightforward to solve. Since the voltages are functions of  $w_0$ , the generated power can be calculated by assuming the harvester is connected to a resistor:

$$P = \frac{V^2}{R} \quad [44]$$

The  $w_0$  in [32] are in even order and hence the third order equation gives three solutions. By solving the equation for intra-well and inter-well cases, we will obtain two sets of solutions, which correspond to two modes of oscillations (Figure 3). The jumps and tilt of the two curves show clearly the two modes of oscillations have characteristic softening and stiffening frequency responses. The softening response tilts to lower frequencies, which can be used for low-frequency energy harvesting at low g's. When the input excitation is strong enough, the beam can snap between two buckled positions and the inter-well oscillation is triggered. The stiffening response has shifted up low-frequency response, which has large amplitude and increases the power output at low frequencies. The analytical solutions have been compared to the numerical integration results at 0.5 g and 3 g (Figure 4). The governing

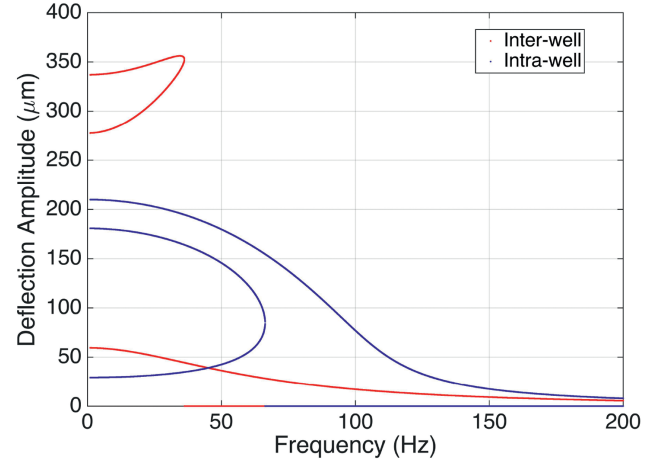


**Figure 3:** Simulated frequency response of bi-stable oscillator. The blue and red lines are the solutions of intra-well and inter-well oscillations respectively. The simulation is based on the meso-scale model parameters shown in Figure 5 with acceleration amplitude of 1 g.

equations have been integrated numerically from 0 to 1 s with initial conditions as the system has the lowest energy (buckled position, zero velocity). The numerical amplitude has been extracted from the maximum and minimum after half a second (assumed steady). The two modes of oscillations and power enhancement have also been verified by experiment.

## Experimental Validation

In order to validate the lumped parameter model and simulation obtained from harmonic balance analysis, a meso-scale experimental setup has been built as shown in Figure 5. The tested prototype has a stainless steel sheet (57.6 mm × 20.2 mm × 0.2 mm) as the structural layer, which is pre-compressed to buckle and then clamped at both ends (the manual pre-compression can be easily implemented in macro scale, while for the MEMS device, manual compression is not feasible and compression is introduced by the residual stresses in thin films). A circular tungsten proof mass (21.9 g, diameter: 19 mm, thickness: 4 mm) is attached at the center of the beam. To transduce the mechanical vibration in electrical signal, two PZT fiber-based energy harvesters (*Smart Materials Corp.*, material properties could be found in Smart-material.com and 'MFC' (2015); PZT fiber as the piezoelectric layer, and epoxy covering the PZT as the passivation layer) were glued by epoxy (*3M DP460*) on the steel sheet on both sides of the proof mass. The energy harvesters were directly connected to a load resistor of

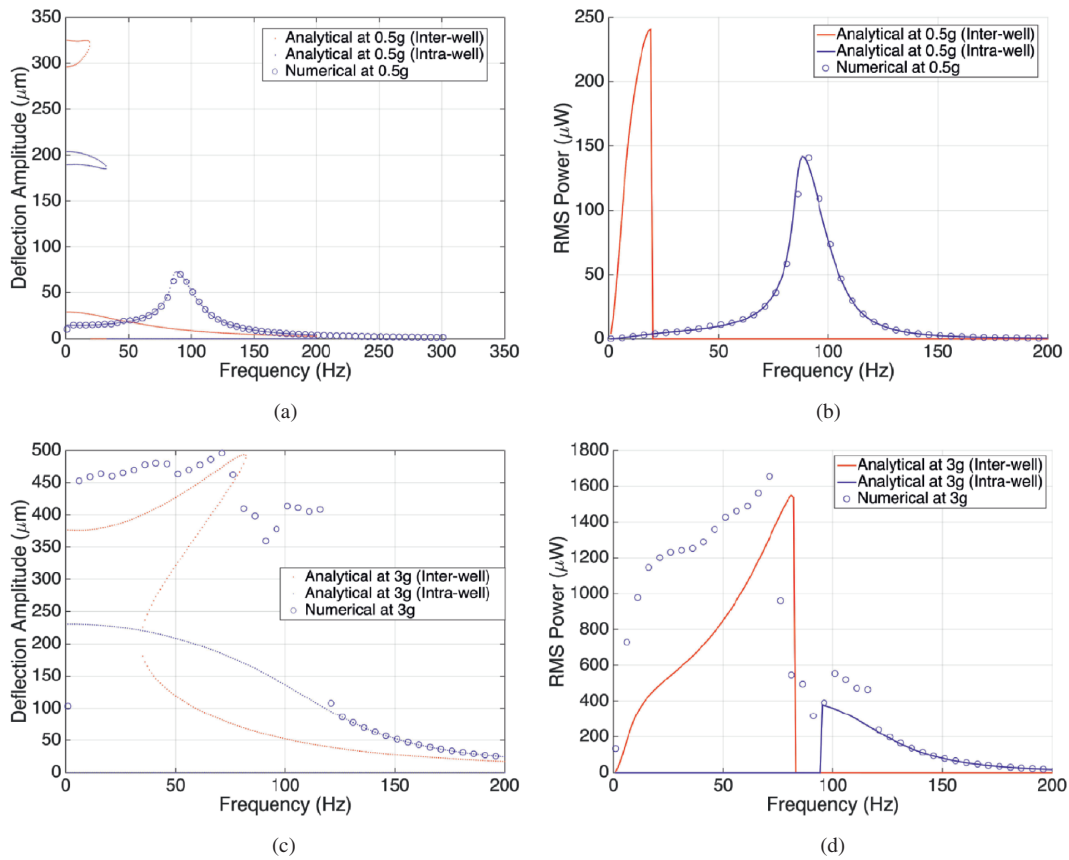


**Figure 4:** Comparison between analytical solutions and numerical integration solutions. (a) and (b) compares the deflection and power in frequency domain at low excitation amplitude of 0.5 g so that the harvester oscillates intra-well. (c) and (d) compares the deflection and power in frequency domain at 3 g so that the harvester oscillates inter-well.

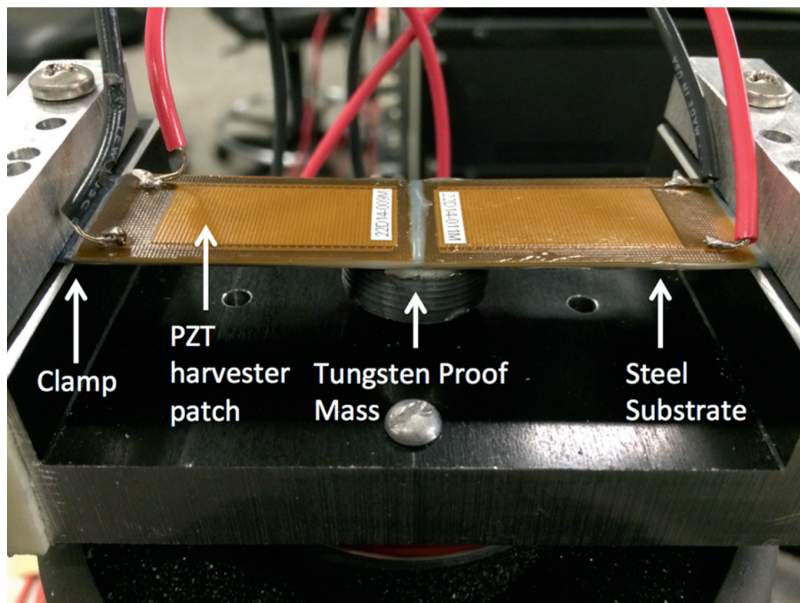


**Figure 5:** A photo of the tested structure mounted on the electromagnetic shaker. The clamped-clamped beam consists of a steel sheet of  $57.6 \text{ mm} \times 20.2 \text{ mm} \times 0.2 \text{ mm}$  as the elastic substrates and two PZT fiber-based energy harvester patches. The center tungsten proof mass is 21.9 g.

2 M $\Omega$  for power generation measurement. The device is mounted on an electromagnetic shaker (*Labworks ET-126*) for vibration testing. The vibration is monitored by an accelerometer (*Analog Devices ADXL335*), and the frequency and amplitude were controlled real-time on *LabVIEW (v11.01)*. Sweeping the excitation frequency at fixed amplitude has been done to generate frequency response.

By using the same device, the bi-stable configuration (pre-compressed to buckling) and mono-stable configuration (without pre-compression) were tested at high input acceleration amplitude of 3 g to compare the stiffening responses. The RMS power generation has been measured and plotted in Figure 6. It is clear that the bi-stable system jumps up from 60 Hz to 70 Hz while the mono-stable configuration has not. The jump down for both configurations were not reached due to the required g-input was too high for the testing setup. The shifted jump made bi-stable configuration generate more power than the mono-stable configuration at low frequencies.

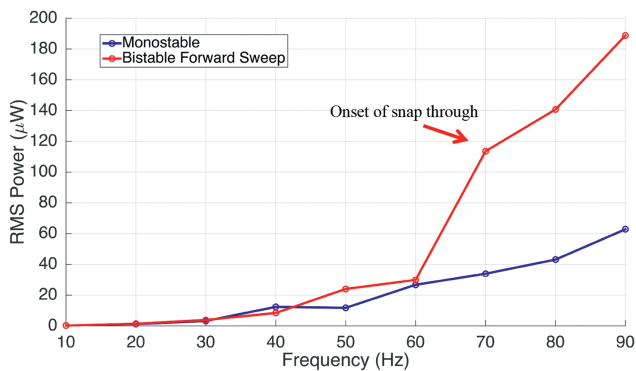


**Figure 6:** RMS power responses of mono-stable and bi-stable configurations. The testing was carried out at 3 g for the same beam in two configurations. It is clear that the bi-stable system outputs higher power at lower frequencies. The jump-down has not been reached due to the limit of the shaker.

The bi-stable and mono-stable configurations have also been tested at low input acceleration amplitude of 1 g. The input acceleration amplitude was set well below the critical amplitude so that inter-well oscillation could not be triggered. Figure 7 compares the bi-stable response and the response of the mono-stable system. As predicted by the analytical model, the bi-stable configuration has softening response at low g's. The jump up during forward frequency sweep and jump down during backward frequency sweep clearly shows the hysteresis. The softening response generates higher power with even wider bandwidth than the mono-stable response.

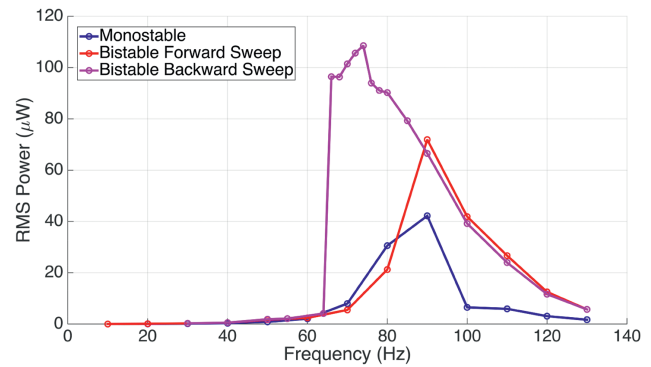


**Figure 7:** Comparison of the softening response of the bi-stable configuration and the mono-stable configuration. The testing was done by sweeping the frequency up and down slowly at 1 g. Jump up and jump down clearly show the hysteresis. Compared to the mono-stable configuration, the softening response of the bi-stable configuration even produces more power with wider bandwidth.

The inter-well mode of the bi-stable energy harvester is a preferred design target since it generates much higher power than the intra-well mode. The intra-well softening response could also be possible employed at low excitation amplitude. To exploit the higher hysteresis branch showed in sweeping frequency testing in real vibrations, controlled actuation may be needed (Hajati 2010). When designing bi-stable energy harvesters, the targeting frequency range should match the frequency range from jump-up to jump-down frequencies, for either inter-well mode or intra-well mode operation. A MEMS scale mechanical bi-stable oscillator is currently fabricated and will be tested to further verify the design concepts and modeling.

## Conclusion

A lumped model with electromechanical coupling has been built for the nonlinear bi-stable beam based piezoelectric energy harvester using Lagrange's formulation. With residual stress and multi-layer beam structure built in, this model applies particularly to residual stress induced post-buckled clamped-clamped beam made by MEMS fabrication. The lumped parameters as functions of system parameters are obtained by assuming the beam vibrates at the first buckling mode. By adopting the harmonic balance method and assuming appropriate harmonic functions, we approximate the frequency responses of the two modes of oscillations analytically. The analytical solutions agree well with the numerical integration results. A meso-scale prototype has been built, and tested in

frequency domain at low and high excitation amplitudes. The enhancements of the power generation compared with mono-stable configuration validate the analytical model.

**Acknowledgement:** The author would like to thank the MIT-SUTD International Design Center for funding this research.

## References

- Arrieta, A. F., et al. 2010. "A Piezoelectric Bi-Stable Plate for Nonlinear Broadband Energy Harvesting." *Applied Physics Letters* 97:104102.
- Arrieta, A. F., et al. 2013a. "Broadband Vibration Energy Harvesting Based on Cantilevered Piezoelectric Bi-Stable Composites." *Applied Physics Letters* 102:173904.
- Arrieta, A.F., et al. 2013b. "Modelling and Configuration Control of Wing-Shaped Bi-Stable Piezoelectric Composites Under Aerodynamic Loads." *Aerospace Science and Technology* 29:453–461.
- Betts, D. N., et al. 2012. "Optimal Configurations of Bistable Piezo-Composites for Energy Harvesting." *Applied Physics Letters* 100:114104.
- Betts, D. N., et al. 2013. "Investigation of Bistable Piezo-Composite Plates for Broadband Energy Harvesting." *Proc. SPIE 8688, Active and Passive Smart Structures and Integrated Systems*.
- Cottone, F, et al. 2012. "Piezoelectric Buckled Beams for Random Vibration Energy Harvesting." *Smart Materials and Structures* 21 (3):035021.
- Erturk, A, and D. J Inman. 2011. "Broadband Piezoelectric Power Generation on High-Energy Orbits of the Bistable Duffing Oscillator with Electromechanical Coupling." *Journal of Sound and Vibration* 330 (10):2339–2353.
- Hajati, A. 2010. "Ultra Wide-Bandwidth Micro Energy Harvester," Doctoral Thesis, Massachusetts Institute of Technology, 2010.
- Hajati, A, and S.-G Kim. 2011. "Ultra-Wide Bandwidth Piezoelectric Energy Harvesting." *Applied Physics Letters* 99 (8):083105.
- Inman, D. J. 2011. *Piezoelectric Energy Harvesting*, 247–256. New York: John Wiley & Sons Ltd.
- Jung, S.-M, and K.-S Yun. 2010. "Energy-Harvesting Device with Mechanical Frequency-up Conversion Mechanism for Increased Power Efficiency and Wideband Operation." *Applied Physics Letters* 96 (11):111906.
- Mann, B. P, and B. A Owens. Apr. 2010. "Investigations of a Nonlinear Energy Harvester with a Bistable Potential Well." *Journal of Sound and Vibration* 329 (9):1215–1226.
- Qiu, J, J. H Lang, and A. H Slocum. Apr. 2004. "A Curved-Beam Bistable Mechanism." *Journal of Microelectromechanical Systems* 13 (2):137–146.
- Smart-material.com, 'MFC'. 2015. [Online]. Accessed October 1, 2015. <http://www.smart-material.com/MFC-product-main.html>.
- Standards Committee of the IEEE Ultrasonics, Ferroelectrics. 1988. "An American National Standard IEEE Standard on Piezoelectricity."
- Stanton, S. C, C. C McGehee, and B. P Mann. 2010. "Nonlinear Dynamics for Broadband Energy Harvesting : Investigation of a Bistable Piezoelectric Inertial Generator." *Physica D* 239 (10):640–653.
- Taki, M. S, Tikani, R, S. Ziaei Rad, and A. Firouzian Nejad. 2016. "Dynamic Responses of Cross-Ply Bi-Stable Composite Laminates with Piezoelectric Layers." *Archive of Applied Mechanics* 86 (6):1003–18.
- Xu, R, and S.-G Kim. 2015. "MEMS Energy Harvesting From Low-Frequency and Low-G Vibrations." *MRS Proceedings* 1782:9–14.